Supporting Information

Wu *et al.* 10.1073/pnas.0802788105

SI Text

Protein Labeling Protocol. The protein used in the labeling reaction was freshly dialyzed from ammonium sulfate precipitates with standard 10 mM potassium phosphate/0.2 mM EDTA (pH 7.8)/buffer, which was degassed and flushed thoroughly with nitrogen. For labeling purposes, 1 mM βME was replaced with TCEP. The protein was diluted to a final concentration of 1 mg·ml^{-1}. A 10-fold molar excess of 1,5-IAEDANS (Invitrogen) was added drop-wise to initiate the labeling reaction. The reaction was left in the dark for 2 h at room temperature, and then an extra batch of 10-fold molar excess IAEDANS was added for an additional 2 hours at room temperature. The reaction was stopped by addition of a 10-fold excess of DTT and unreacted dye was removed by thorough dialysis. The labeling ratio was quantified by comparing the absorption spectrum of labeled protein with unlabeled protein using extinction coefficients of ε_{278} = 18,200 M^{-1}cm^{-1} for αTS, ε_{278} = 1,100 M^{-1}cm^{-1}, and ε_{334} = 5,700 M^{-1}cm^{-1} for IAEDANS and further verified by mass spectroscopy. Typical labeling efficiency was 90%.

Distance Distribution Analysis by Nonlinear Least Squares Analysis Using Analytic Gaussian Functions. The Gaussian distribution analysis was carried out as described (1, 2). The donor-only and donor–acceptor time-resolved fluorescence decays were globally fit to an analytic function described by Eq. **S1**. The pair distribution function assumes an explicit form:

$$I_d(t) = \sum_i^N \alpha_i e^{-k_{di}\cdot t} + \text{constant}$$

$$I_{da}(t) = \int_0^\infty I_d(t)\cdot p(k_{ET})\cdot e^{-k_{ET}\cdot t}\cdot dk_{ET} \qquad \textbf{[S1]}$$

where α is the amplitude of the decay component with rate k_d, k_{ET} is the energy transfer rate and $p(k_{ET})$ is the energy transfer rate distribution. All of the donor subpopulations giving rise to the different rates were assumed to have the same energy-transfer rate distribution. The energy transfer rate distribution, $p(k_{ET})$, is related to the pair distance distribution, $p(r)$, according to the Förster equation:

$$r^6 = R_0^6\cdot\left(\frac{k_{d_{ave}}}{k_{ET}}\right) \qquad \textbf{[S2]}$$

where $k_{d_{ave}}$ is the inverse of the average lifetime of the donor in the absence of the acceptor. The distribution $p(k_{ET})$ is described by a Gaussian distribution function:

$$p(r) = \sum_i a_i e^{-(r-\omega_i)^2/2\sigma_i^2} \qquad \textbf{[S3]}$$

where a_i is a normalized amplitude, ω_i the center, and σ_i the width of the ith Gaussian. The width of the Gaussian was converted to the full-width at half-maximum (FWHM) by the following relationship:

$$\text{FWHM} = \sigma/2.354 \qquad \textbf{[S4]}$$

A standard Marquardt–Levenberg nonlinear least-squares global-fitting algorithm was used to perform the fits. The instrument response for each curve was taken into account by iterative reconvolution with the calculated decay curve. The donor excited state decay was best fit by using a three-exponential model for both the 15-212 and 168-212 data at all folding time points. These rates were held fixed during the subsequent global analyses. The donor-only and donor–acceptor data for each kinetic folding-time point were fit to a single- and double-Gaussian function. To obtain better model discrimination between these two models, a global fit of all of the donor-only and donor–acceptor data was carried out. The double-Gaussian fit gave a statistically more significant improvement in the fit (improvement in reduced χ^2 by more than a factor of 2 with 5,700 degrees of freedom) and exhibited dramatically more random residuals. The local reduced χ^2 of each decay trace was comparable in the results of the local and global fits, suggesting that the amplitudes rather than the peak position and width of the Gaussian functions are changing with folding time. For data that could be fit locally to a double-Gaussian function (e.g., the first four datasets in Fig. 4; the amplitude of the smaller peak was too small in the fifth dataset), the peak positions were consistent with those obtained from the global fit.

Distance Distribution Analysis Using Laplace Inversion via The Maximum Entropy Method (MEM). For time-resolved kinetics, Kumar *et al.* (3) have shown that the distribution of decay rates can be accurately recovered using MEM. Application of MEM to time-resolved FRET requires analysis of both the donor and the donor–acceptor excited state decays. The analysis is analogous to MEM analysis of time-resolved anisotropy (4). The donor excited-state decay was described according to Eq. **S5**:

$$I_d(t) = \int_0^\infty p(k_d)e^{-k_d\cdot t}\,dk_d \qquad \textbf{[S5]}$$

$$k_d \equiv \frac{1}{\tau_d}$$

where k_d is defined, for convenience, as the inverse of the donor lifetime and $p(k_d)$ is the distribution of donor excited state decay rates. For the donor–acceptor-labeled system, the excited-state decay was given as

$$I_{da}(t) = \int_0^\infty\int_0^\infty p(k_d, k_{ET})e^{-(k_d+k_{ET})\cdot t}\,dk_d dk_{ET} \qquad \textbf{[S6]}$$

where k_{ET} is the energy transfer rate given by the Förster equation. The 2D distribution $p(k_d,k_{ET})$ describes the distribution of donor rates and energy-transfer rates. The distribution $p(k_d,k_{ET})$ is usually approximated in 1D analyses as separate 1D distributions giving rise to a "nonassociative"model:

$$I_{da}(t) = \int_0^\infty p(k_d)e^{-k_d\cdot t}\,dk_d\cdot\int_0^\infty p(k_{ET})e^{-k_{ET}\cdot t}\,dk_{ET} \qquad \textbf{[S7]}$$

This assumption assumes that every subpopulation responsible for a different donor rate has the same energy-transfer rate distribution. The pair distance distribution was then calculated from the rate distribution according to the Förster equation (2). Although this approximation results in significant computational advantages, the underlying assumptions are not generally applicable. For example, a partially folded state and the unfolded

state may be equally populated, and the donor may exhibit different excited-state lifetimes and a different donor–acceptor distance in each state. Because the discrimination of these subpopulations was one of the goals of our FRET studies, we have analyzed the data using the 2D distribution with Eq. **S6** instead of Eq. **S7**. The Gaussian distribution analysis also assumes a separation of variables as in Eq. **S7**, and therefore fewer assumptions are made in the MEM analysis.

Software. Our 2D-MEM package, coded in LabVIEW 8.2 (National Instruments), incorporates procedures described (3, 4). The implementation consisted of extending the standard MEM algorithm to analyze two datasets simultaneously (4). In practice, the distribution $p(k_d,k_{ET})$ was represented as a 32×32 or 40×40 grid of rates in logarithmic rate space. In the MEM optimization the 2D grid of amplitudes was collapsed into a 1D array. The same amplitudes were used for the donor and donor–acceptor data, with additional terms for labeling efficiency and for normalization of protein concentration. The results were not sensitive to typical uncertainties of several percent in the determination of protein concentration. Even a significant error in this normalization was tolerable because an underestimate of the donor–acceptor-labeled sample concentration results in a δ-function energy-transfer rate at the highest possible rate, which was easily identified and did not affect the rest of the distribution. The program is also able to independently adjust this parameter, but the results presented in this article had this parameter fixed to the known value. The apparent rate, k_{app}, of the excited-state decay, $I(t)$, was given as follows:

$$I(t) = \int_0^\infty \int_0^\infty p(k_d, k_{ET}) e^{-k_{app}t}\, dk_d\, dk_{ET}. \qquad \textbf{[S8]}$$

$$k_{app} = k_D \text{ (donor only);}$$

$$k_{app} = k_D + k_{ET} \text{ (donor–acceptor).}$$

Other than this modification, the maximum entropy analysis followed the approach suggested by Kumar *et al.* This implementation avoided the occurrence of degeneracies in the amplitudes ("iso-kappa" curves in ref. 4). An instrument response for each decay trace was taken into account by aperiodic convolution with the decay rate matrix. Although not used in the results presented here, the software contains additional terms to account for scattered light and an infinite time offset.

The approach successfully resolves the donor and the energy transfer rate distributions for synthetic data, especially for high FRET efficiencies. At low FRET efficiencies (<10–15%), the peak positions and high-efficiency tails are reproduced accurately, but the low-efficiency tails of the distributions extend slightly beyond that of the input synthetic data. The ability of the analysis to accurately identify subpopulations and their peak positions in a completely model-independent manner makes it a useful complement to the Gaussian analysis and a useful tool for analysis of time-resolved FRET data.

1. Haran G, Haas E, Szpikowska BK, Mas MT (1992) Domain motions in phosphoglycerate kinase: determination of interdomain distance distributions by site-specific labeling and time-resolved fluorescence energy transfer. *Proc Natl Acad Sci USA* 89:11764–11768.
2. Lakowicz J (1999) *Principles of Fluorescence Spectroscopy* (Plenum Publishers, New York).
3. Kumar ATN, Zhu LY, Christian JF, Demidov AA, Champion PM (2001) On the rate distribution analysis of kinetic data using the maximum entropy method: Applications to myoglobin relaxation on the nanosecond and femtosecond timescales. *J Phys Chem B* 105:7847–7856.
4. Gallay J, Sopkova J, Vencent M (2000) in *Topics in fluorescence spectroscopy*, ed. Lakowicz J (Kluwer Academic/Plenum Publishers, New York).

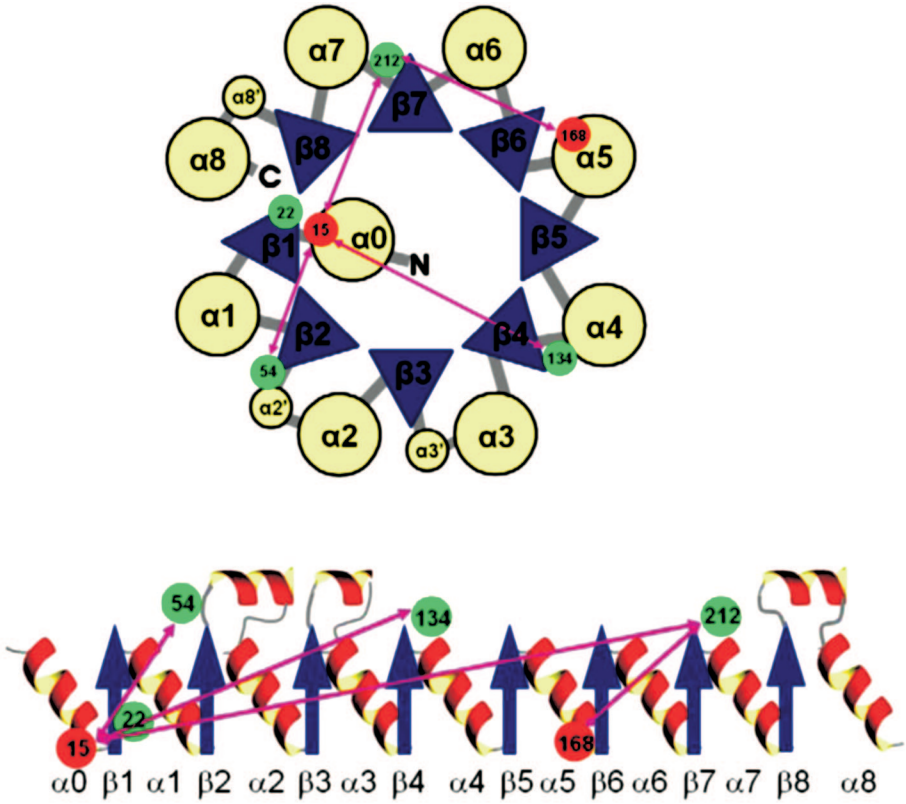

Fig. S1. Top-view (*Upper*) and side-view (*Lower*) topology map of αTS illustrating the location of the FRET probes. The Trp residues (donors) are shown as green circles, and the Cys residues labeled with IAEDANS are shown as red circles. The single-tryptophan variants with W22 (F22W) and W212 (F212W) serve as local structural probes in time-resolved anisotropy assays. W22 was not used in the FRET studies.

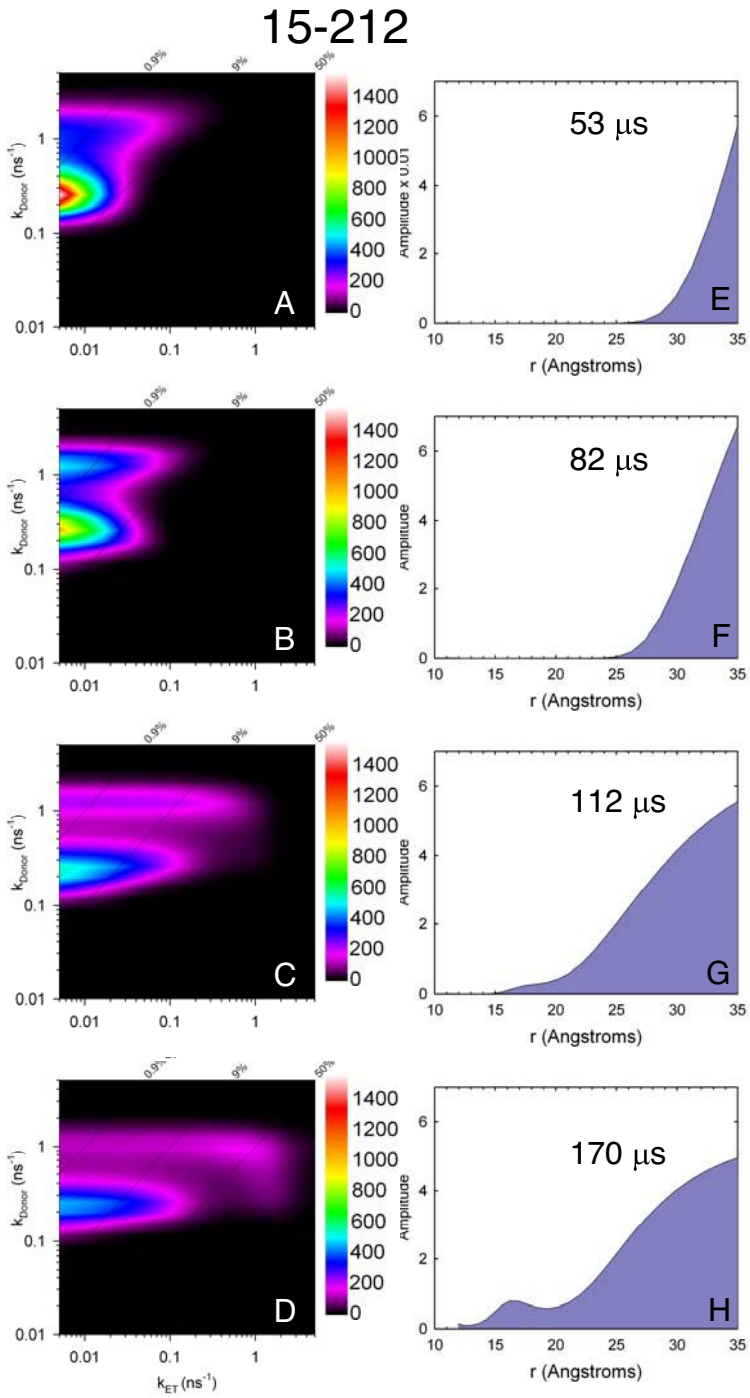

Fig. S2. Energy transfer rate distributions as a function of donor excited state decay rate for the 15-212 FRET pair obtained from global 2D Laplace inversion by MEM of donor-only and donor–acceptor time-resolved fluorescence traces. (*A–D*) A contour plot of the energy-transfer rate, k_{ET}, for each donor rate component, $k_D = 1/\tau_D$, is shown at various refolding times: 53 μs (*A*), 82 μs (*B*), 112 μs (*C*) and 170 μs (*D*). The dotted diagonal lines in the (k_D, k_{ET}) projection corresponding to FRET efficiencies, $E_{FRET} = k_{ET}/(k_D + k_{ET})$, of 0.9%, 9%, and 50% are also shown. (*E–H*) The corresponding EED distributions calculated for cross-sections with $k_D = 0.25$ ns^{-1} using the Förster equation with $R_o = 22$ Å and $\kappa^2 = 2/3$ are shown. Based on the measured anisotropy of W212 (Fig. 5) and estimated anisotropy of AEDANS, values of κ^2 can range between 0.4 and 1.5, however, leading to an uncertainty in the distances of approximately ±10%.

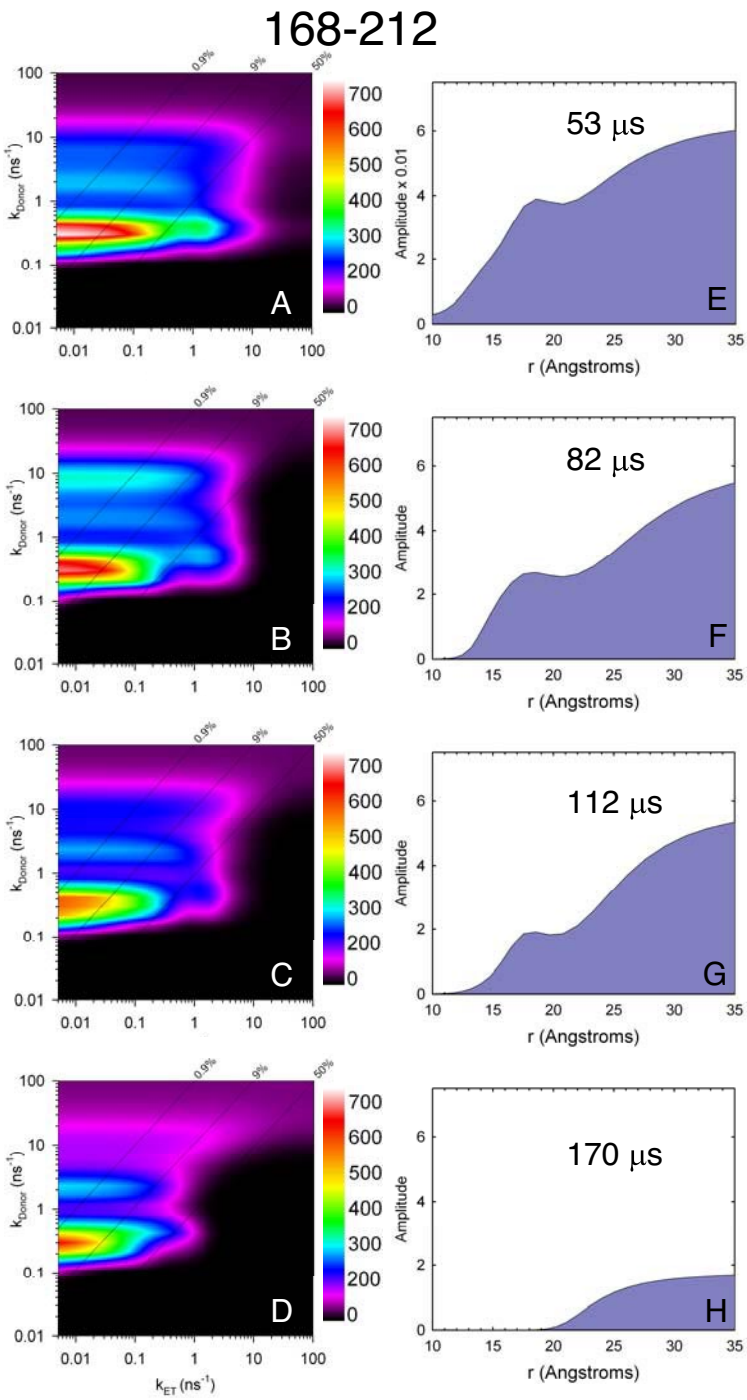

Fig. S3. Energy transfer rate distributions as function of donor excited state decay rate for the 168-212 FRET pair obtained from global 2D Laplace inversion by MEM of donor-only and donor–acceptor time-resolved fluorescence traces. Descriptions are the same as in Fig. S2 except the EED distributions are calculated for cross-sections with $k_D = 0.42\ ns^{-1}$.

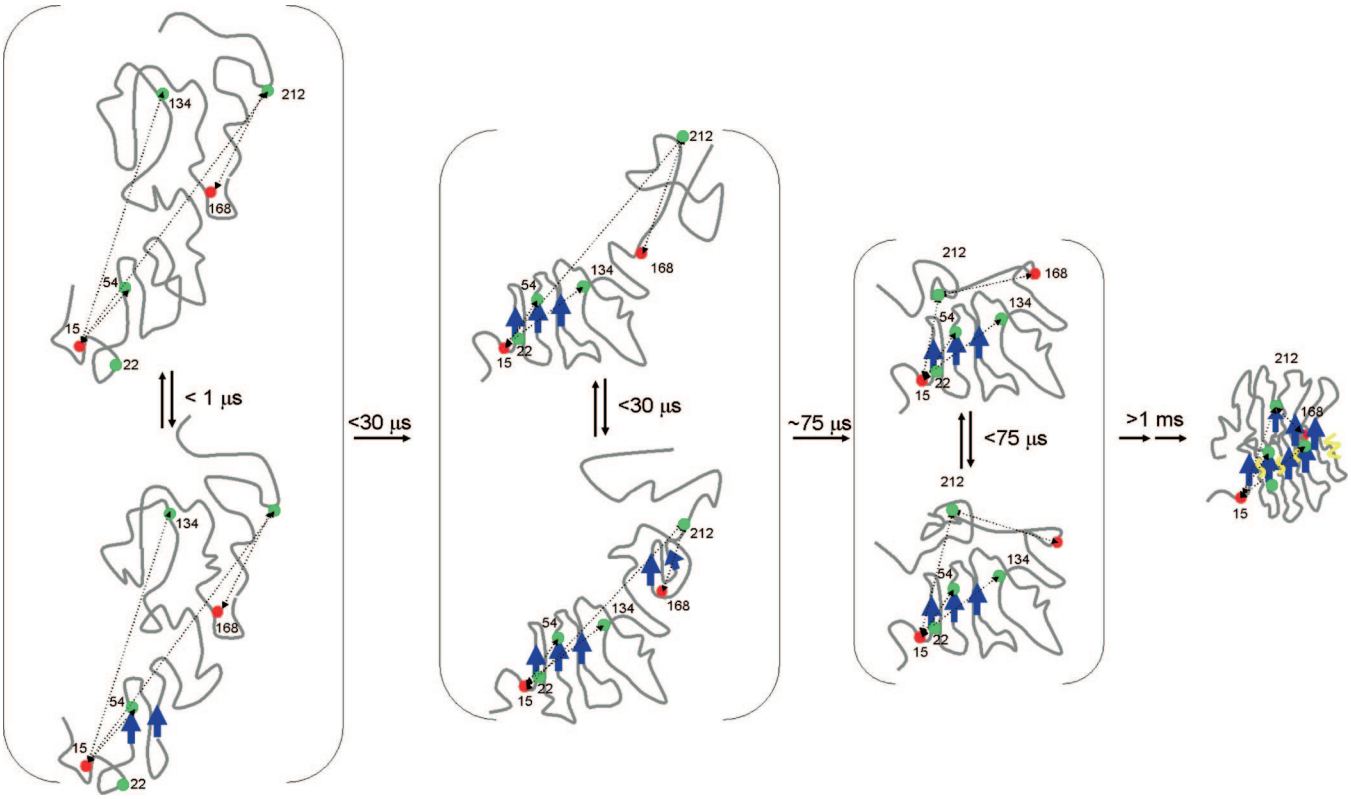

Fig. S4. Cartoon schematic of the early folding events of αTS. The $<$30-μs and $>$1-ms kinetic steps occur outside the detection window of the continuous-flow mixer. The brackets denote an equilibrium between the (possibly off-pathway or misfolded) compact conformations and the more extended conformations detected in the continuous-flow FRET experiments for the 15-212 and 168-212 pairs.

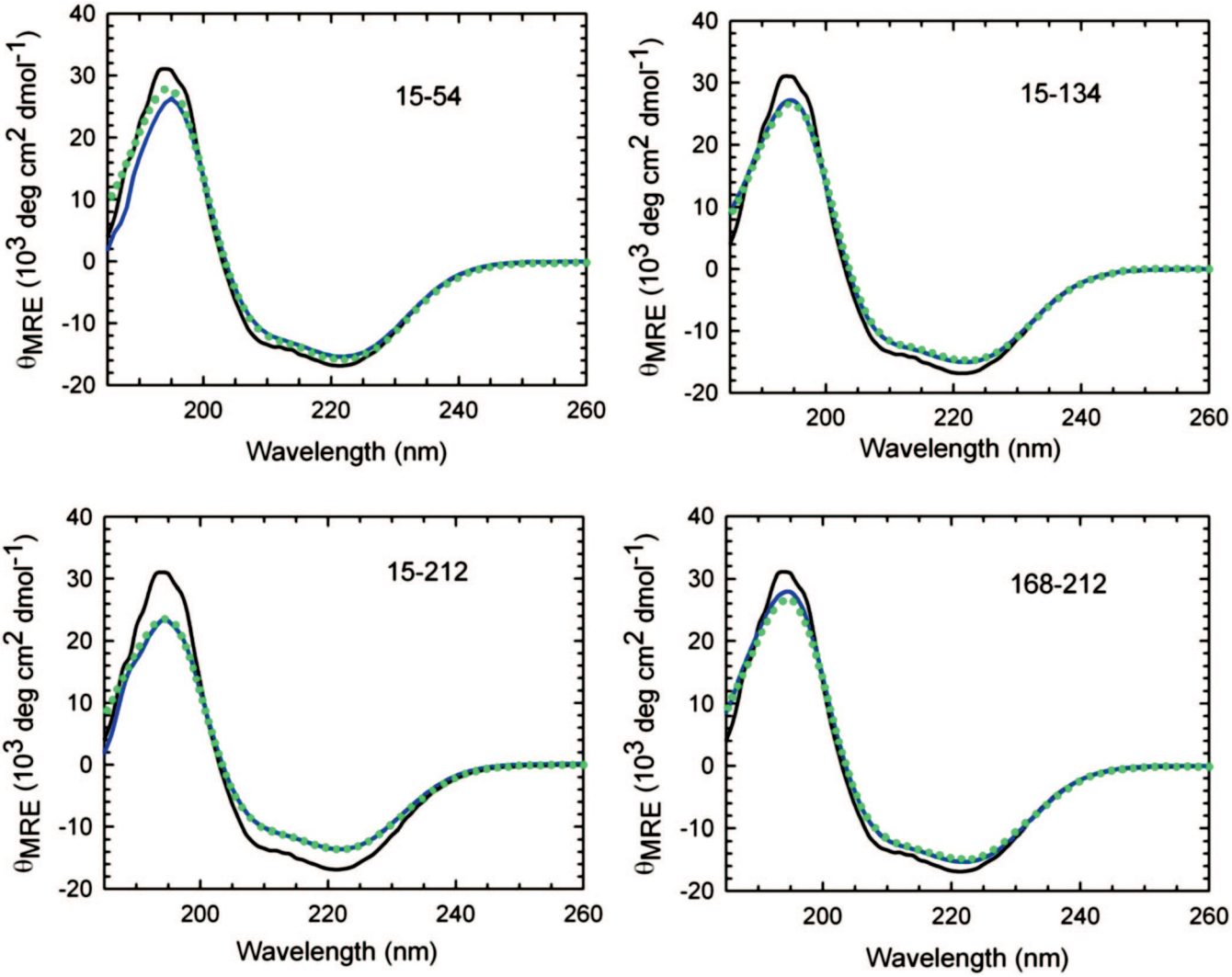

Fig. S5. CD spectra of variants used in the trFRET study. The native-state CD spectrum of the variants with and without the AEDANS acceptor are shown as a dotted green line and a solid blue line, respectively. The native-state spectrum for the WT (solid black line) is shown for reference. All spectra were recorded at 25°C in 10 mM phosphate buffer containing 0.2 mM K_2EDTA and 1 mM βME.

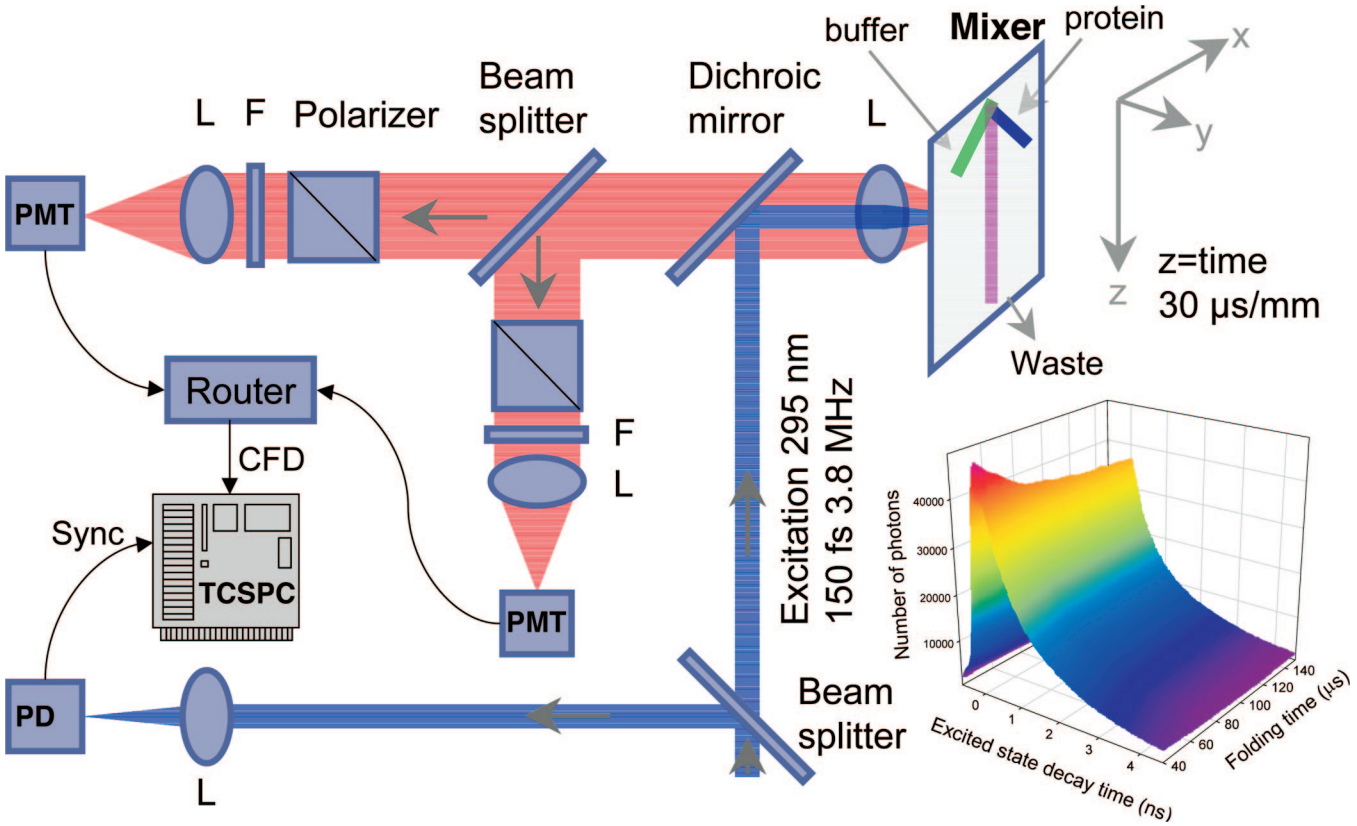

Fig. S6. Experimental setup for performing continuous-flow experiments with time-resolved FRET and time-resolved anisotropy detection. L, 50-mm focal length plano-convex lens; F, 350-nm band-pass filter; PMT, photomultiplier tube (PMH100; Becker–Hickl); PD, fast photodiode; CFD, constant-fraction discriminator; Sync, synchronization pulse; TCSPC, time-correlated single photon-counting board (SPC630; Becker–Hickl). The *Inset* shows a typical dataset of time-resolved fluorescence decays (nanosecond time-scale axis) as a function of folding time (microsecond folding-time axis).